




Cite this: *Phys. Chem. Chem. Phys.*,
2021, **23**, 24579

Photoluminescence of monolayer MoS₂ modulated by water/O₂/laser irradiation†

Chao Hou,^a Jingwen Deng,^a Jianxin Guan,^a Qirong Yang,^a Zhihao Yu,^a Yilin Lu,^b Zihan Xu,^c Zefan Yao^a and Junrong Zheng *^a

The low photoluminescence (PL) quantum yields of transition metal dichalcogenide monolayers have been a limiting factor for their optoelectronic applications. Various and even inconsistent mechanisms have been proposed to modulate their PL efficiencies. Herein, we use PL/Raman microspectroscopy and the corresponding *in situ* mapping, atomic force microscopy, and field-effect transistor (FET) characterization to investigate the changes in the structural and optical properties of monolayer MoS₂. Relatively low power density ($<4.08 \times 10^5 \text{ W cm}^{-2}$) of laser irradiation in ambient air can cause a slight PL suppression effect on monolayer MoS₂, whereas relatively high power density ($\sim 1.02 \times 10^6 \text{ W cm}^{-2}$) of laser irradiation brings significant PL enhancement. Experiments under different atmospheres reveal that the laser-irradiation-induced enhancement only occurs in the atmosphere containing O₂ and is more remarkable in pure O₂. In addition, physically adsorbed water can also induce PL enhancement of monolayer MoS₂. FET devices suggest that the adsorbed water produces a p-doping effect on MoS₂, and the laser irradiation in ambient air generates an n-doping effect, and both types of doping can enhance the PL intensity. The island-shaped defects caused by laser irradiation can be stabilized by oxygen atoms and act as trapping centers for excited trions or electrons, thus reducing the non-radiative recombination ratio and enhancing the PL intensity. The physically adsorbed water works in a similar way. A low power density of laser irradiation can sweep away the originally adsorbed H₂O on the surface, thus reducing the PL.

Received 9th August 2021,
Accepted 11th October 2021

DOI: 10.1039/d1cp03651c

rsc.li/pccp

1 Introduction

Atomically thin transition metal dichalcogenides (TMDCs) have drawn increasing attention due to their unique properties.¹ Compared to the conventional semiconductors, the reduced screening and strong electron–hole interactions in monolayer MoS₂ and its analogs (MoSe₂, WS₂, WSe₂, etc.) make them spectrally robust and amenable to various optoelectronic devices such as field-effect transistors,² light-emitting devices,³ and solar cells.⁴ Monolayer MoS₂ and its heterostructures with other two-dimensional (2D) monolayers are also emerging as novel platforms for studying many-body effects.^{5,6} The interactions among phonons, photons, and charged quasiparticles determine their fundamental properties, *e.g.*, photoluminescence (PL), heat generation, and charge

separation and transport. It has been shown that the density of surface defects (*e.g.*, vacancies, impurities, dislocations, and grain boundaries) on exfoliated MoS₂ reaches 8% of the total area, which causes variations in conductivity, Fermi level position, and stoichiometry across very small areas.^{7–9} On the as-grown monolayer MoS₂ *via* the chemical vapor deposition (CVD) method, more defects may appear due to the complex chemical reaction process. The abundant defects, acting as efficient electron traps, affect its electron mobility and optical properties.¹⁰

Although MoS₂ monolayers have many excellent properties, its low PL quantum yield (typically much smaller than 1%), which originates from the slow spontaneous radiative recombination of optically generated electrons and holes,¹¹ has severely limited its optoelectronic applications. Recently, various approaches have been developed to enhance the PL performances of TMDC monolayers, including chemical treatment,^{12–15} thermal annealing,^{16–18} chemical doping,¹⁹ surface plasmonic effects^{20,21} and laser irradiation.^{22–24} However, the reported enhancement effects vary significantly and sometimes are inconsistent even when using the same method.^{25,26} Many mechanisms have been proposed to explain the PL enhancement. One popular interpretation is repairing sulfur

^a College of Chemistry and Molecular Engineering, Beijing National Laboratory for Molecular Sciences, Peking University, Beijing 100871, China.
E-mail: junrong@pku.edu.cn

^b Institutes of Physical Science and Information Technology, Anhui University, Hefei 230601, China

^c Shenzhen Sixcarbon Technology, Shenzhen 518106, China

† Electronic supplementary information (ESI) available: Fig. S1–S10 cited in the main text. See DOI: 10.1039/d1cp03651c

vacancies by laser modification,^{22,24,27} or by some chemical molecules, such as super acid,^{12,26} hydrohalic acid,¹³ methanol,¹⁴ and thiol-group-containing molecules,¹⁵ which can eliminate the defect-mediated nonradiative recombination. Another interpretation is the n/p-doping on the monolayers through the adsorption of solution-based n/p-type chemicals¹⁹ and through the thermal-^{16,17} or laser-^{23,28} assisted charge transfer from O₂ and H₂O in the atmosphere, which switches the dominant PL process from trions with a low radiative recombination rate to the neutral excitons with a high radiative recombination rate. The PL enhancement was also reported to be implemented by a simple electrostatic doping method.²⁹ The enhancement of PL by plasmonic nanostructures is proposed due to the plasmon-enhanced adsorption of the excitation laser as well as the charge transfer between the metal and TMDC monolayers.^{20,21} Besides, the quenching of PL intensity by oxygen plasma treatment is believed to be associated with the creation of MoO₃ disordered defects leading to a direct-to-indirect bandgap transition.³⁰

Herein, we systematically explore the PL modulations of monolayer MoS₂ by 532 nm laser irradiation under well-controlled conditions, aided with characterization methods such as PL/Raman microspectroscopy and atomic force microscopy (AFM) imaging, and field-effect transistor (FET) devices. Owing to different defects at different sites on the same sample and the sensitivity of the optical properties of monolayer MoS₂, we use *in situ* treatment and measurement in the PL/Raman characterization to guarantee the accuracy of the results.

2 Experimental

2.1 Sample preparation

Monolayer MoS₂ triangular domains were grown in a two-temperature-zone furnace through the CVD method. MoO₃ powder (Alfa Aesar, 99.999%, 0.01 g) as the precursor was placed downstream with 30 cm from sulfur powder (Alfa Aesar, 99.999%, 0.3 g). A clean Si wafer with a 285 nm SiO₂ top layer was placed face down at 3 cm downstream from the crucible containing MoO₃ powder. 300 sccm Ar gas was utilized as the carrier gas. After purging Ar gas for 20 min, the temperature for MoO₃ and sulfur powders was increased to 650 °C and 180 °C, respectively. Then the monolayer MoS₂ triangles were obtained after 7 min of growth.

2.2 PL/Raman microspectroscopy and spectra acquisitions

In this work, we used our home-built PL/Raman microspectroscope to control and measure the optical properties of monolayer MoS₂ accurately. As displayed in Fig. 1a, there is a partial overlap between the optical microscope path and the signal acquisition path. The overlapped optical microscope path includes an LED, a convex lens and a beam splitter, which will be flipped down when acquiring signals *via* flip mount adapters. The PL/Raman signals were collected using a liquid-nitrogen-cooled EMCCD camera through the monochromator (Andor Shamrock SR-303i). We used a shutter to precisely control the laser irradiation time. The effect of the atmosphere on the optical properties of MoS₂ was investigated using our

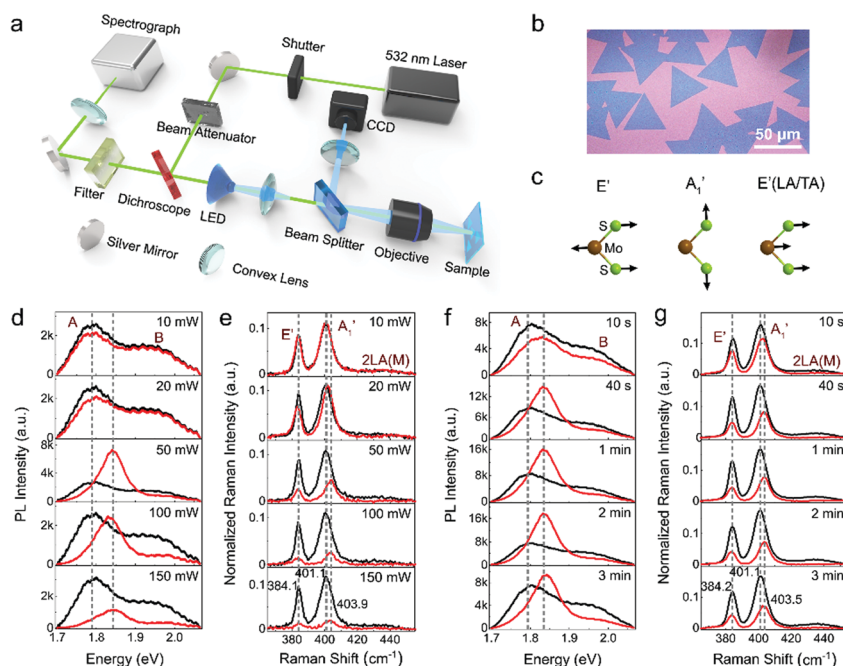


Fig. 1 (a) Optical setup of the home-built PL/Raman microspectroscope. (b) Optical image of the as-grown monolayer MoS₂ on the SiO₂/Si substrate. (c) Symmetry and normal displacements of the three optical vibration modes discussed in this work for monolayer MoS₂. (d) PL and (e) Raman signals of monolayer MoS₂ before (black curve) and after (red curve) laser irradiation for two minutes with various laser powers. (f) PL and (g) Raman signals of monolayer MoS₂ before (black curve) and after (red curve) laser irradiation with 50 mW for different times. Spectra in (d–g) are taken with an excitation power of 5 mW for 10 s. Raman signals in e and g are normalized to the peak at 520 cm⁻¹ of the Si/SiO₂ substrate.

own designed atmosphere controllable cell shown in Fig. S1 (ESI[†]). In order to maintain the focus state of the laser on the sample unchanged, we adapted a flexible hermetic bag to build the atmosphere controllable cell. Air with high humidity (H₂O atmosphere) was created by using a humidifier. PL and Raman single point spectra for the MoS₂ were acquired in a stable air environment (17–20 °C, with humidity 10–30%). A solid-state laser diode (532 nm) was used as the excitation and laser treatment source. The laser was focused through a 50× long-working-distance objective lens (0.7 NA) providing a spot size of about 2.5 μm. The typical excitation power was 5 mW, and the integration time was 10 s. We used 600 gr mm⁻¹ grating and 300 μm slit to obtain PL spectra but used 1800 gr mm⁻¹ grating and 50 μm slit to acquire Raman spectra.

2.3 PL/Raman mappings and AFM measurement

PL and Raman mappings were obtained by using a commercially available confocal Raman microscopic system (HR Evolution, HORIBA Jobin Yvon) equipped with a 532 nm laser and 100× objective lens. The focused laser spot size on the sample was around 0.6 μm. Gratings of 600 gr mm⁻¹ and 1200 gr mm⁻¹ were adapted for PL and Raman mappings, respectively. The mapping step size is 0.5 μm with swift-on mode, and the integration time on each point is 0.5 s. All mappings were achieved using 10% laser power at room temperature in ambient air. The thickness and topographical variations in the samples were examined with the tapping mode by using a commercial atomic force microscope (AFM, NSK, SPI3800/SPA400).

2.4 Fabrication and characterization of FET devices

Polymethyl methacrylate (PMMA, Microchem, 495 K, A6) was first spin-coated onto the sample as the mask. High-resolution electron beam lithography was then conducted to expose an area designed by Auto CAD to remove the samples within 200 × 200 μm area around the desired MoS₂ single domain. Next, the exposed areas were etched through a precise oxygen plasma etching process, followed by a subsequent rinse with acetone to remove the top PMMA layer. Similarly, second lithography was performed to create the source and drain electrode patterns. Subsequently, Cr/Au (5 nm/45 nm) electrodes were thermally evaporated onto the substrate, and the PMMA mask was removed. Finally, the device was annealed in a vacuum at 200 °C for 3 h to eliminate PMMA residuals and any moisture. The electrical characterization of MoS₂ FET devices were carried out in ambient air at a probe station using a Keithley 4200 SCS as the parameter analyzer.

3 Results and discussion

3.1 Laser irradiation can suppress or enhance the PL of monolayer MoS₂

Fig. 1a illustrates the layout of a home-built PL/Raman microspectroscope, which is the primary characterization tool in this work. It provides better flexibility for controls under

experimental conditions than a commercial counterpart. The samples used in the experiments are single-crystal monolayer MoS₂ (Fig. 1b). The triangular-shaped MoS₂ monolayers have a uniform size of ~45 μm. The unit cell of monolayer MoS₂ consists of three atoms with nine normal phonon modes (three acoustic and six optical modes) at the Γ point in the Brillouin zone. In this work, we monitor the in-plane optical vibrational mode E', out-of-plane optical mode A₁', and the in-plane acoustic mode E'(LA/TA), which are described in Fig. 1c to evaluate the structural change in monolayer MoS₂ upon laser and gas molecule treatments.

Fig. 1d displays the PL spectra of the MoS₂ monolayer before (black curves) and after (red curves) 532 nm laser irradiation for two minutes with different powers in ambient air. The PL spectrum has two broad peaks A and B. After irradiation with low power (e.g., 10 and 20 mW, with a focus spot of ~2.5 μm), the intensity of peak A decreases slightly. When the laser power increases to 50 mW, the PL intensity increases sharply by about three times. The prominent peak (peak A) position blue-shifts about 50 meV and its line shape becomes narrower. However, if the laser power continues to increase to 100 and 150 mW, the intensity of peak A starts to diminish with its central energy remaining at the blue-shifted position. The perplexing power dependent PL modulation suggests that the laser-irradiation-induced modification is not monotonic and is the comprehensive result of several molecular mechanisms playing their roles together.

The *in situ* Raman measurements of the monolayer MoS₂ before (black curves) and after (red curves) laser irradiation are shown in Fig. 1e. There are three peaks in the spectra, corresponding to different vibrational modes illustrated in Fig. 1c. The two prominent peaks (E' at ~384 cm⁻¹ and A₁' at ~401 cm⁻¹) belong to the first-order Raman scattering, and the very weak peak (~437 cm⁻¹) denoted as 2LA(M) is assigned to a second-order longitudinal phonon mode at M point in the Brillouin zone.³¹ With irradiation at a relatively low power (e.g., 10 mW), the Raman peaks' positions and intensities hardly change. When the power reaches 50 mW, the intensities of the Raman peaks are considerably reduced. In the meantime, the A₁' mode has an obvious blue-shift (~2.8 cm⁻¹), whereas the position of E' remains almost unchanged. If the power increases beyond 50 mW, the Raman intensities continue to diminish with the peak positions remaining at ~384.1 cm⁻¹ and the blue-shifted at ~403.9 cm⁻¹, respectively. The reduced intensities suggest damage occurs. The optical images before and after laser treatments of different powers (Fig. S2, ESI[†]) also show the structural damage when the power reaches and is higher than 50 mW. This phenomenon reveals that with certain structural alteration, the PL of the monolayer MoS₂ can be enhanced. Nevertheless, if the structure is damaged too much, the PL is suppressed.

Similarly, with a fixed power of 50 mW, the PL spectra of the monolayer MoS₂ are obtained (Fig. 1f) by tuning the laser irradiation time. Even a laser processing time of 10 s can cause the blue-shift of peak A. And the enhancement of peak A reaches its maximum value (~2.4 times) with a two-minute

irradiation. The corresponding Raman spectra (Fig. 1g) indicate that the laser irradiation of 50 mW as short as 10 s still induces a remarkable reduction in the Raman intensities. Similar to the results of tuning laser power, the position of E' mode remains unchanged, and the A_1' mode blue-shifts for $2\text{--}3\text{ cm}^{-1}$ on tuning the irradiation time. The optical images (Fig. S3, ESI[†]) reveal that structural damages occur with 50 mW power for any irradiation time. We also try to use lower power (10 mW and 20 mW) of laser to irradiate the sample for long enough time (e.g., 15 minutes). However, we cannot see any enhancement in its PL performance, and there is no detectable structural change under a microscope, either. It is to be noted that the above procedures *via* tuning powers and irradiation times have been repeated many times on different samples to ensure the repeatability of the results.

3.2 The suppression of PL signals can be reversible and the enhancement is irreversible

To investigate whether the changes in PL and Raman signals caused by laser irradiation are reversible or not, we store the samples in ambient air (relative humidity $\sim 15\%$) after being irradiated with 20 mW and 50 mW power for two minutes, respectively, and then the signal evolution was monitored within 25 hours (Fig. S4, ESI[†]). As can be seen, for the sample irradiated with 20 mW power (Fig. S4a and b, ESI[†]), both PL and Raman signals gradually increase with time, and after ~ 25 hours finally return to their respective initial values before laser irradiation. The signal change is much faster within the first two hours. During the 25 hours, no obvious changes are observed in optical images (Fig. S4c, ESI[†]). The results indicate that the PL and Raman changes are reversible, implying that a power of 20 mW laser probably only blows away physically adsorbed impurities (e.g., H_2O , O_2 , etc.) on the surface rather than causing permanent structural damage to the monolayer MoS_2 . Without the adsorbed impurities, the PL intensity is attenuated. After reabsorbing the impurities from air, the PL intensity is restored. This reasoning immediately leads to at least three further directions to explore: (1) if the laser power is sufficiently high to cause structural damage to MoS_2 , the PL and Raman signal changes should be irreversible; (2) what are

the major components of impurities that cause both PL and Raman signal changes? (3) why can the impurities cause the PL/Raman changes? In the following, experiments are conducted to investigate these issues. The experimental results with a laser power of 50 mW are displayed in Fig. S4d–f (ESI[†]). After storing in ambient air for 25 hours, the PL and Raman signals cannot restore to their initial values. Structural damage to MoS_2 caused by the high power is clearly visible in the optical images. This is distinctly different from the lower power case discussed above (Fig. S4a–c, ESI[†]).

3.3 Effects of laser irradiation on monolayer MoS_2 revealed by *in situ* PL/Raman mappings and AFM

A more detailed insight into the variations of monolayer MoS_2 properties after laser processing is provided by spatial PL and Raman mappings (Fig. 2). We use a commercial Raman microscope with a high spatial resolution ($\leq 600\text{ nm}$) of the mapping function to conduct the *in situ* laser scanning process and compare the mappings before and after laser irradiation. We select 25%, 50%, and 100% power of the instrument to scan the sample. Considering the $\sim 0.6\text{ }\mu\text{m}$ laser spot for the commercial instrument, 100% power ($\sim 1.59 \times 10^6\text{ W cm}^{-2}$) is basically equivalent to the power density of 50 mW ($\sim 1.02 \times 10^6\text{ W cm}^{-2}$) for our own equipment ($\sim 2.5\text{ }\mu\text{m}$ laser spot). By analogy, 50% ($\sim 7.95 \times 10^5\text{ W cm}^{-2}$) corresponds to 20 mW ($\sim 4.08 \times 10^5\text{ W cm}^{-2}$), and 25% ($\sim 3.98 \times 10^5\text{ W cm}^{-2}$) corresponds to 10 mW ($\sim 2.04 \times 10^5\text{ W cm}^{-2}$). The power density adapted by the commercial instrument is generally higher than that by using our own one. This is because during the laser scanning process using the commercial instrument, the focused laser remains at each point on the sample only for 0.5 s, much shorter than using our own setup.

After using 25%, 50% and 100% power of 532 nm *in situ* laser irradiation, the structural damage only occurs within 100% power treated area (Fig. 2a and b). Fig. 2c shows the PL mapping profiles of intensity, peak position, and full width at half maximum (FWHM) for emission peak A. As can be seen, there is no detectable difference in the area irradiated by 25% power. In the 50% power treated area, the intensity of peak A drops, coupled with the red-shifted peak position and enlarged

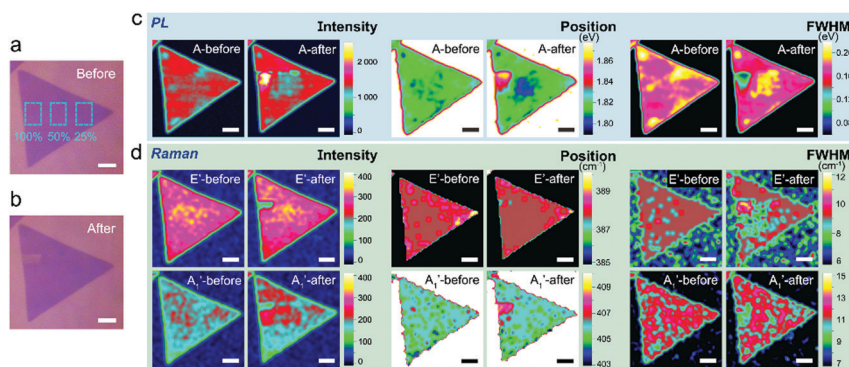


Fig. 2 Optical images of the monolayer MoS_2 triangle domain (a) before and (b) after laser irradiation with 25%, 50%, and 100% power, respectively. (c) PL and (d) Raman mappings of the intensity, peak position, and FWHM for A emission peak, and E'/A_1' mode, respectively. Scale bars are all $5\text{ }\mu\text{m}$.

FWHM. In the 100% power treated region, a huge enhancement and an evident blue-shift of peak A are observed, together with shrinking FWHM. The corresponding Raman mapping profiles are shown in Fig. 2d. At the locations treated by 25% and 50% power, the two Raman modes E' and A_1' have almost no change. With 100% laser power treatment, the intensities of both Raman peaks are reduced in the damaged region shown in Fig. 2b, along with the hardly changed position of E' mode and blue-shifted A_1' mode. These PL and Raman changes after different powers of laser treatments are well consistent with those results conducted by using our home-built apparatus. The average single-spot PL/Raman spectra corresponding to different laser-treated regions are shown in Fig. S5 (ESI[†]) for comparison. Since different samples are used and the Raman spectra/mappings cannot be normalized by 520 cm^{-1} of the SiO_2/Si substrates, the relative intensities and positions of the PL/Raman peaks are slightly different from those measured in Fig. 1.

The effect of laser treatment time is studied using 100% power at different regions for different treatment times on the same MoS_2 triangular domain. The optical images (Fig. 3a and b) suggest more laser processing times leading to more structural damages. Among the four laser-treated regions, the area where laser treatment is performed three times has the largest amplitude of PL enhancement, the largest blue-shifted peak position and the most reduced FWHM (Fig. 3c). The following Raman mappings (Fig. 3d) indicate a good correlation between the intensity profile for E' mode and the optical image (Fig. 3b) after laser treatment, with lower intensity at more severely damaged regions. In addition, the position of the E' mode slightly red-shifts, whereas the position of the A_1' mode remarkably blue-shifts. The FWHMs of both modes change little after laser processing. The average single-spot PL/Raman spectra corresponding to each area are illustrated

in Fig. S6 (ESI[†]). AFM mapping is performed to investigate the changes in morphology and thickness of monolayer MoS_2 . As shown in Fig. 3e, the surface of pristine monolayer MoS_2 (denoted as number 0) is not perfectly flat, and the measured thickness is larger than the theoretical value (0.65 nm) of monolayer MoS_2 owing to the adsorbed impurities on the surface. The thickness is reduced after each laser treatment, and after being irradiated four times, the thickness (0.51 nm) is even smaller than the theoretical value, indicating the structural damage. This reduced thickness may be caused by the evaporation of S resulting from the thermal effect of laser irradiation. As mentioned below in Section 3.6, although some missing S can be occupied by O, the final thickness is still less than the theoretical value.

The results by using 50% power for different times are displayed in Fig. S7 (ESI[†]). As expected, peak A is reduced after 50% power processing, and it is reduced the most within the area treated four times. The corresponding average single-spot PL/Raman spectra are exhibited in Fig. S8 (ESI[†]). Interestingly, although the treated areas do not show significant changes in the optical images (Fig. S7b, ESI[†]), its corresponding AFM images (Fig. S7e, ESI[†]) clearly show every boundary of the areas irradiated by laser scanning. The thickness of monolayer MoS_2 decreases after each time of laser scanning. However, the thickness is always larger than the theoretical value. This demonstrates that the laser irradiation with 50% power does not damage the structure of the MoS_2 . Considering the results of the experiments under high humidity air discussed in the next part, the most likely reason for the slight PL suppression here is the laser irradiation with 50% power only sweeps away the adsorbed H_2O on the surface of the sample in ambient air.

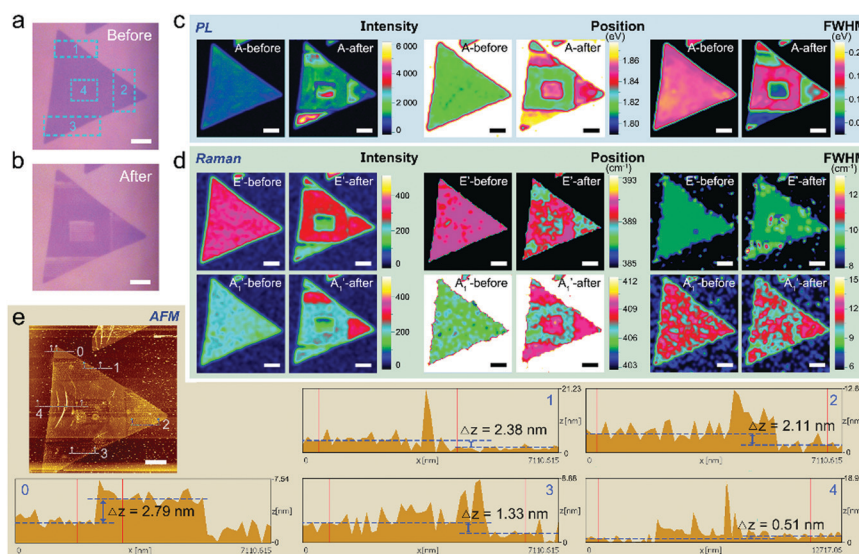


Fig. 3 Optical images of the monolayer MoS_2 triangle domain (a) before and (b) after laser irradiation with 100% power for once, twice, three times and four times, respectively. (c) PL and (d) Raman mappings of the intensity, peak position, and FWHM for A emission peak, and E'/A_1' mode, respectively. (e) The corresponding AFM results after laser treatment. Numbers 0 denotes the area before treatment. Number 1–4 represent areas after laser treatment with 100% power for once, twice, three and four times, respectively. Δz reveals the thickness of the corresponding area. Scale bars are all $5\ \mu\text{m}$.

3.4 Different atmospheres produce different effects

The above experiments suggest that molecules adsorbed on the MoS₂ surface play important roles. We then design an atmosphere controllable cell (Fig. S1, ESI[†]) assembled to our home-built instrument to carry out *in situ* PL/Raman measurements under different atmospheres: pure N₂, Ar, O₂, or air with high humidity (relative humidity 90–98%). Fig. 4a shows the PL spectra of monolayer MoS₂ before laser irradiation in ambient air (black curves), and before (blue curves)/after (red curves) laser irradiation (50 mW for 2 minutes) in different gas atmospheres. For clarity, Fig. 4b lists the intensity, position, and FWHM of peak A corresponding to each PL spectrum in Fig. 4a. As shown in panel N₂, when the atmosphere is switched from ambient air (black curve) to pure N₂ (blue curve), peak A is reduced in intensity and has a slight redshift in position. This may arise from the fact that N₂ blows away the originally adsorbed H₂O molecules in ambient air, which is similar to the effect of low power of laser irradiation in Fig. 1d and Fig. S7 (ESI[†]). After laser treatment in pure N₂ (red curve), the intensity of peak A decreases significantly, and the peak position slightly blue-shifts. The results are very similar to those in pure Ar (panel Ar in Fig. 4a). Unlike in air, no PL enhancement is observed in N₂ or Ar with various laser power densities and irradiation times. N₂ and Ar are relatively inert and interact weakly with MoS₂. The PL enhancement observed in air (panel air in Fig. 4a) must be caused by molecules with more active properties.

Panel O₂ in Fig. 4a displays the results under an O₂ atmosphere. Without laser irradiation, there is no distinct change in the PL spectra after adding pure O₂ (blue curve) compared to that measured in air (black curve). Following the laser treatment in pure O₂, the intensity of peak A increases by ~3.8 times, which is even larger than that treated in ambient air (~2.4 times). The presence of water also increases the PL intensity (panel H₂O in Fig. 4a). Without laser treatment, peak A is enhanced by ~2.0 times once the humidity in the air is increased from 10–20% (black curve) to 90–98% (blue curve). After being irradiated by laser in H₂O-rich air (red curve), the

intensity of peak A decreases back. The observations indicate that adsorbing water can enhance the PL and removing the surface water by laser irradiation can reduce the PL intensity. In general, the positions of the original PL spectra (black curves) are different because different samples have different originally doped states. For the magnitudes of the peak-shift after laser treatment, they are obviously smaller in N₂ and Ar than those in other atmospheres under the same excitation conditions.

The corresponding Raman spectra are shown in Fig. 4c–e. After laser treatments in different atmospheres, the two Raman peaks (red curves) decrease dramatically, indicating structural damage to MoS₂. Besides, the A₁' mode has a significant blue-shift, while the E' mode has a relatively smaller red shift. Before laser irradiation, the adsorption of H₂O molecules (the blue curve under an H₂O-rich atmosphere) can also cause a remarkable blue-shift of the A₁' mode. The intensity of the A₁' mode becomes stronger at the same time. Similar Raman changes of the monolayer MoS₂ after interaction with H₂O molecules are also reported recently by Tumino et al.³² In general, the magnitudes of the peak-shift after laser treatment for the two modes are larger in N₂ and Ar than in other atmospheres. This indicates that the O₂/H₂O can stabilize the defects from such damage. The optical images of the sample before and after laser treatments in different atmospheres are shown in Fig. S9 (ESI[†]). We can see that the laser irradiation destroys the monolayer's structure in any of the atmospheres.

The above experiments prove that the surface water adsorption can increase the PL intensity, and the laser damage in the presence of O₂ can both increase the PL intensity and significantly change the PL line shape.

3.5 The FET device and AFM image reveal the surface condition of monolayer MoS₂ after laser irradiation

The PL intensity of MoS₂ is correlated with its carrier concentration.^{29,33} A FET device is fabricated to explore the n/p doping effect caused by laser treatment and water adsorption. As displayed in Fig. 5a and b, the FET device is treated with laser irradiation (50 mW, 2 minutes) in ambient air at

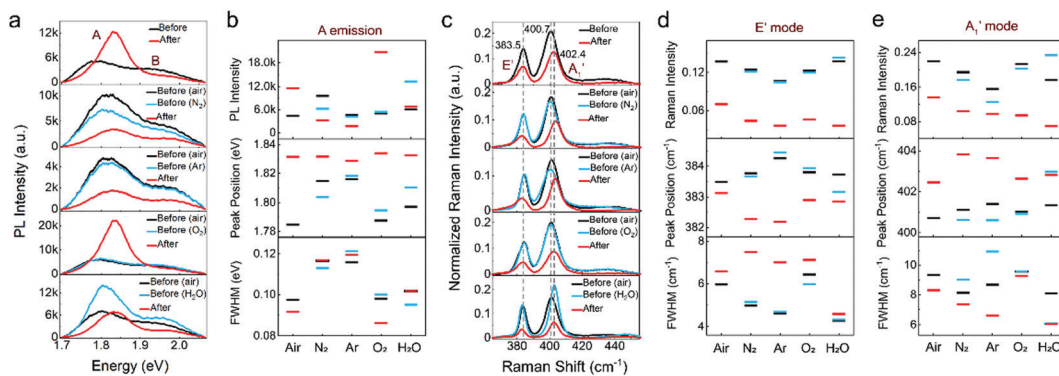


Fig. 4 (a) PL and (c) Raman spectra of monolayer MoS₂ before laser irradiation in ambient air (black curve), before (blue curve) and after (red curve) laser irradiation (50 mW for 2 minutes) in different atmospheres (from top to bottom): ambient air (with humidity 10–20%), N₂, Ar, O₂, and H₂O (with humidity 90–98% in ambient air). All the spectra are taken with an excitation power of 5 mW for 10 s. Raman signals in (c) are normalized to the peak at 520 cm⁻¹ of the Si/SiO₂ substrate. Stacking of intensity, peak position, and FWHM for (b) A emission peak, and for (d) E' mode and (e) A₁' mode.

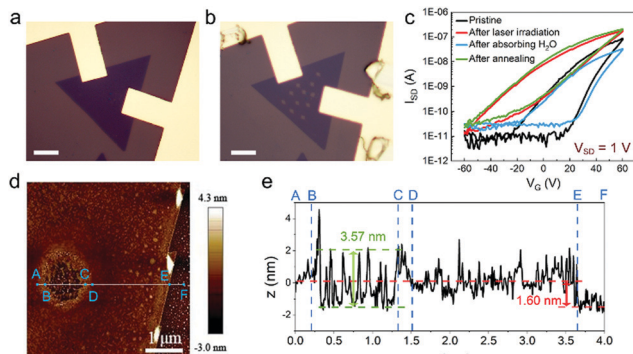


Fig. 5 Optical images of the monolayer MoS₂ FET device (a) before and (b) after laser irradiation at several sites on the surface. (c) Source–drain current (I_{SD}) versus back gate voltage (V_G) curves with a source–drain voltage (V_{SD}) of 1 V recorded from the device before treatment (black curve), after laser irradiation (red curve), then adsorbing H₂O molecules (blue curve), and subsequently annealing at 200 °C for 3 h in a vacuum (green curve), respectively. (d) The AFM image and (e) the corresponding line profile showing one site after being irradiated by laser. Scale bars in a and b are 10 μ m.

multiple points within the current channel. The source–drain current (I_{SD}) versus back gate voltage (V_G) curves taken under various processing conditions are shown in Fig. 5c. The laser irradiation turns the already n-type monolayer MoS₂ (black curve) into more n-type (red curve), with an increase in the conductance and a shift of threshold voltage. This result is contrary to the enhanced mechanism proposed in the literature^{22,27} which states the enhancement is caused by laser-assisted p-type doping to MoS₂. After adsorbing H₂O molecules in air with high-humidity, the electron concentration decreases sharply (blue curve), verifying that the physically adsorbed H₂O molecules have a p-doping effect on MoS₂. Once the adsorbed water evaporates by annealing in the vacuum, the

transfer characteristics (green curve) are basically restored to the last state of being irradiated by laser (red curve). The p-doping effect by adsorbing water will disappear after annealing or laser irradiation with relatively low power, confirming that it is a physical adsorption. In contrast, suitable laser irradiation in an atmosphere containing O₂ produces an n-doping effect, which is an irreversible chemical change. Both the n-doping and p-doping effects enhance the PL.

Fig. 5d shows the AFM image of one site after being irradiated by laser. It shows the rugged surface within the laser irradiated spot. The corresponding line scan (Fig. 5e) reveals that the fluctuation range within the hole is \sim 3.57 nm which is obviously higher than that in the pristine monolayer MoS₂ (\sim 1.60 nm). This phenomenon is not so obvious in the situation of PL mapping *in situ* laser treatment in Fig. 3, due to the different irradiation methods and conditions. The fact in Fig. 5d demonstrates that the laser irradiation produces many defects on the monolayer MoS₂. The effects to the PL change will be discussed in the following section.

3.6 Power dependence of laser-treated signals and the mechanisms of PL enhancement

Before the mechanisms of PL enhancement are discussed, we should consider the influence of excitation laser power on the formations of various excitons in MoS₂. Fig. 6a shows a schematic view of the electronic band structure of monolayer MoS₂, denoting multiple types of quasiparticles.^{34–36} Excitons A and B originate from the direct-gap transitions between the conduction and valence bands at the *K*-points. The energy difference between excitons A and B comes from the valence band splitting due to the strong spin–orbital interaction. Since charged excitons (*i.e.*, trions) are easy to form because of enhanced Coulomb interaction in the monolayer structure, the schematic diagram highlights trion A[−] (usually negative type in as-grown

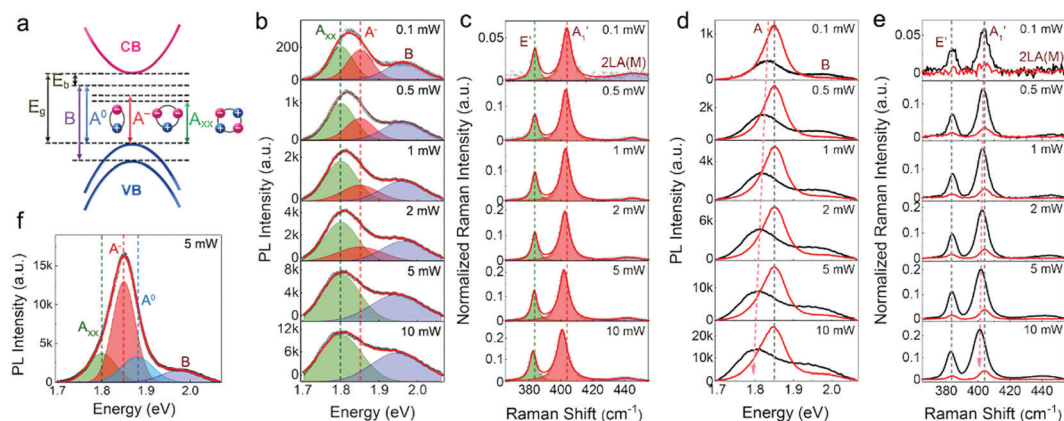


Fig. 6 (a) Schematic of direct-gap transitions at *K*-point in monolayer MoS₂ (the higher spin-split conduction band is not shown). The associated A, B excitons, negative trions (A[−]), biexciton (A_{xx}), the bandgap E_g , and the binding energy E_b of exciton A are illustrated. (b) PL and (c) Raman spectra of pristine monolayer MoS₂ taken in ambient air with different laser excitation powers (0.1–10 mW). Each PL spectrum in (b) is fitted with Gaussian peaks (A_{xx}, A[−], and B). Each Raman spectrum in (c) is fitted with Lorentz peaks for E', A₁' and 2LA(M) modes. (d) PL and (e) Raman spectra of monolayer MoS₂ before (black curves) and after (red curves) laser irradiation (50 mW, 2 mins) taken in ambient air excited with different powers (0.1–10 mW). (f) The fitted PL spectrum after laser irradiation (the red curve of panel "5 mW" in d) with Gaussian peaks. The spectra acquisition times are all 10 s. Raman signals in c and e are normalized to the peak at 520 cm^{−1} of the Si/SiO₂ substrate.

MoS₂) to distinguish it from neutral exciton A⁰. With relatively high excitation laser power, the biexciton (denoted as A_{xx}) peak becomes dominant in the PL spectrum because of the high carrier concentration. To investigate the excitation power dependence of the PL/Raman spectra, we use different laser powers (0.1–10 mW, that is 2.04×10^3 to 2.04×10^5 W cm⁻²) to excite the same position of the as-grown monolayer MoS₂. As displayed in Fig. 6b, the PL spectra can be decomposed into four Gaussian peaks: biexciton A_{xx} (1.80 eV), trion A⁻ (1.85 eV), neutral exciton A⁰ (1.88 eV), and exciton B (1.95–1.98 eV). There are no A⁰ peaks in the fitting of Fig. 6b. We have recorded the A⁰ peak-dominant PL spectrum (Fig. S10a, ESI[†]) with another sample when excessive water is adsorbed and droplets form on the surface. Since we must have high power density of the laser ($\sim 1.02 \times 10^6$ W cm⁻²) to achieve the laser-induced PL enhancement, we have to use the 50 \times objective lens in our instrument. Under this condition, the excitation laser power cannot be adjusted low enough, or the PL signal will be too weak. We realized low excitation power (80 W cm⁻²) using a 10 \times objective lens, turning out the A⁻ peak-dominant PL spectrum (Fig. S10b, ESI[†]) because of the unintentional n-type doping resulted from the sulfur vacancy defects during sample preparation.^{8,37} Back to Fig. 6b, the proportion of A⁻ recombination decreases and A_{xx} gradually dominates the spectrum with the increase of the excitation power. The corresponding Raman spectra, which are analyzed with Lorentz peak-fitting (Fig. 6c), reveal that as the excitation power increases, the A₁' mode red-shifts, and the frequency difference between E' and A₁' mode gradually decreases from 20.1 cm⁻¹ to 18.4 cm⁻¹.

The results of PL performances at the same point but using different excitation laser powers before and after laser irradiation (50 mW, 2 minutes) in ambient air are illustrated in Fig. 6d. With the increase of excitation power, the position of peak A red-shifts (black curves), as shown in Fig. 6b, which is governed by the ratio changes between peaks A_{xx} and A⁻. After laser irradiation, peak A in each PL spectrum (red curves) is significantly enhanced and blue-shifted. Independent of the excitation power, the blue-shifted position of peak A remains constant at ~ 1.85 eV. Fig. 5c reveals that the laser treatment in ambient air results in enhanced n-type doping, suggesting an increased electron concentration in monolayer MoS₂. Taken together, trion A⁻ must always dominate peak A in the PL spectra after laser treatment. This result is verified in Fig. 6f, which shows the fitted result of the red curve in panel “5 mW” in Fig. 6d. The Raman results (Fig. 6e) indicate that independent of the excitation power, the intensities of the two main peaks after laser treatment significantly reduced, and the A₁' mode blue-shifts to almost the same position.

The above results show that the laser-irradiation-induced PL enhancement of monolayer MoS₂ needs both relatively high-power density and the participation of O₂. The relatively high power density of laser causes structural alteration to the MoS₂ monolayer, producing many isolated islands. On the one hand, PL enhancement does not happen without such defects. On the other hand, without O₂ these islands do not lead to

enhancement, either. Raman measurements suggest an interesting explanation for it. The intensities of the two Raman peaks are considerably reduced after laser irradiation (Fig. 4c). The stiffening behavior (blue shift) of the out-of-plane mode (A₁') after laser irradiation can be understood in terms of increasing the restoring force constant perpendicular to the basal plane, as the laser strikes off some of the S atoms at the surface (and some are replaced by O). In the A₁' vibrational configuration, Mo atoms remain fixed and only S atoms vibrate along the *c*-axis (as shown in Fig. 1c), so the disappearance of surface S atoms has a significant influence. In contrast, the relatively stable position of the in-plane vibrational mode E' is because this mode involves vibrations of both Mo and S. Hence the disappearance of surface S atoms has little effect on it. The relatively small peak-shifts for MoS₂ in air and O₂ than that in Ar and N₂ (Fig. 4d and e) demonstrate that the O is bonded to the sample. Because of the bonding with O, the excited electrons and trions are effectively localized at these island-shaped defects, which can significantly suppress the energy dissipation and momentum change resulting from the collisions with other electrons or trions, thus leading to the improved PL signal. In the situation of water-adsorption induced enhancement, the role of adsorbing water is similar to the laser-induced defects. As shown in Fig. S9 (ESI[†]), a small amount of water molecules adsorbed on the surface appear as tiny “particles”. Water is polar and has a dielectric constant much larger than MoS₂, which can solvate electrons, reducing the non-radiative recombination ratio of trions and excitons in MoS₂, thus enhancing the PL.

4 Conclusions

In summary, we have comprehensively controlled and measured the 532 nm laser-treated PL and Raman performances of monolayer MoS₂ by using a home-built instrument as well as a commercial instrument with a mapping function. We find that low power density ($< 4.08 \times 10^5$ W cm⁻²) of laser irradiation in ambient air causes a slight PL suppression to monolayer MoS₂, with almost no change on Raman spectra and optical images. However, relatively high power density ($\sim 1.02 \times 10^6$ W cm⁻²) of laser irradiation in ambient air brings significant PL enhancement with an obvious blue-shift of the energy, together with shallower optical images and reduced Raman peaks. Investigations under different controlled atmospheres demonstrate that the laser irradiation induced enhancement only occurs in the atmosphere containing O₂ and is more remarkable in pure O₂. The adsorption of H₂O molecules without laser function leads to a similar PL enhancement with that caused by laser irradiation in ambient air. The FET devices reveal that the physically adsorbed water leads to p-doping on MoS₂, and the laser irradiation in the presence of O₂ generates the n-doping effect. Both types of doping effects can enhance the PL intensity, so the type of doping is not the key factor for the enhancement. The island-shaped defects caused by laser irradiation can be stabilized by oxygen atoms and act as trapping

centers for excited trions or electrons, thus reducing the non-radiative recombination ratio and enhancing the PL intensity. The physically adsorbed water works in a similar way. And a low power density of laser irradiation can sweep away the originally adsorbed H₂O on the surface, resulting in the PL suppression phenomenon.

Conflicts of interest

There are no conflicts to declare.

Acknowledgements

The work is supported by the National Natural Science Foundation of China (NSFC-21627805, 21804004, and 21821004) and MOST (2017YFA0204702) China. The electrical characteristics of FET devices were determined at Prof. Jian Pei's lab in the college of Chemistry and Molecular Engineering in Peking University.

References

- C. Tan, X. Cao, X.-J. Wu, Q. He, J. Yang, X. Zhang, J. Chen, W. Zhao, S. Han, G.-H. Nam, M. Sindoro and H. Zhang, *Chem. Rev.*, 2017, **117**, 6225–6331.
- X. Lv, W. Wei, P. Zhao, J. Li, B. Huang and Y. Dai, *Phys. Chem. Chem. Phys.*, 2018, **20**, 1897–1903.
- Z. Wang, Q. Jingjing, X. Wang, Z. Zhang, Y. Chen, X. Huang and W. Huang, *Chem. Soc. Rev.*, 2018, **47**, 6128–6174.
- S. B. Kang, K. C. Kwon, K. S. Choi, R. Lee, K. Hong, J. M. Suh, M. J. Im, A. Sanger, I. Y. Choi, S. Y. Kim, J. C. Shin, H. W. Jang and K. J. Choi, *Nano Energy*, 2018, **50**, 649–658.
- X. Wen, H. Chen, T. Wu, Z. Yu, Q. Yang, J. Deng, Z. Liu, X. Guo, J. Guan, X. Zhang, Y. Gong, J. Yuan, Z. Zhang, C. Yi, X. Guo, P. M. Ajayan, W. Zhuang, Z. Liu, J. Lou and J. Zheng, *Nat. Commun.*, 2018, **9**, 1–9.
- H. Liu, Y. Li, Y. S. You, S. Ghimire, T. F. Heinz and D. A. Reis, *Nat. Phys.*, 2017, **13**, 262–265.
- R. Addou, S. McDonnell, D. Barrera, Z. Guo, A. Azcatl, J. Wang, H. Zhu, C. L. Hinkle, M. Quevedo-Lopez, H. N. Alshareef, L. Colombo, J. W. P. Hsu and R. M. Wallace, *ACS Nano*, 2015, **9**, 9124–9133.
- F. Tumino, C. S. Casari, A. L. Bassi and S. Tosoni, *J. Phys. Chem. C*, 2020, **124**, 12424–12431.
- F. Tumino, C. S. Casari, M. Passoni, V. Russo and A. L. Bassi, *Nanoscale Adv.*, 2019, **1**, 643–655.
- Z. Hu, Z. Wu, C. Han, J. He, Z. Ni and W. Chen, *Chem. Soc. Rev.*, 2018, **47**, 3100–3128.
- K. F. Mak, C. Lee, J. Hone, J. Shan and T. F. Heinz, *Phys. Rev. Lett.*, 2010, **105**, 136805.
- M. Amani, D.-H. Lien, D. Kiriya, J. Xiao, A. Azcatl, J. Noh, S. R. Madhupathy, R. Addou, S. Kc, M. Dubey, K. Cho, R. M. Wallace, S.-C. Lee, J.-H. He, J. W. Ager, X. Zhang, E. Yablonovitch and A. Javey, *Science*, 2015, **350**, 1065–1068.
- H.-V. Han, A.-Y. Lu, L.-S. Lu, J.-K. Huang, H. Li, C.-L. Hsu, Y.-C. Lin, M.-H. Chiu, K. Suenaga, C.-W. Chu, H.-C. Kuo, W.-H. Chang, L.-J. Li and Y. Shi, *ACS Nano*, 2016, **10**, 1454–1461.
- G. P. Neupane, M. D. Tran, S. J. Yun, H. Kim, C. Seo, J. Lee, G. H. Han, A. K. Sood and J. Kim, *ACS Appl. Mater. Interfaces*, 2017, **9**, 11950–11958.
- A. Förster, S. Gemming, G. Seifert and D. Tománek, *ACS Nano*, 2017, **11**, 9989–9996.
- H. Nan, Z. Wang, W. Wang, Z. Liang, Y. Lu, Q. Chen, D. He, P. Tan, F. Miao, X. Wang, J. Wang and Z. Ni, *ACS Nano*, 2014, **8**, 5738–5745.
- S. Tongay, J. Zhou, C. Ataca, J. Liu, J. S. Kang, T. S. Matthews, L. You, J. Li, J. C. Grossman and J. Wu, *Nano Lett.*, 2013, **13**, 2831–2836.
- L. Wang, X.-H. Ji, F. Chen and Q.-Y. Zhang, *J. Mater. Chem. C*, 2017, **5**, 11138–11143.
- S. Mouri, Y. Miyauchi and K. Matsuda, *Nano Lett.*, 2013, **13**, 5944–5948.
- Z. Wang, Z. Dong, Y. Gu, Y.-H. Chang, L. Zhang, L.-J. Li, W. Zhao, G. Eda, W. Zhang, G. Grinblat, S. A. Maier, J. K. W. Yang, C.-W. Qiu and A. T. S. Wee, *Nat. Commun.*, 2016, **7**, 1–8.
- J. Huang, G. M. Akselrod, T. Ming, J. Kong and M. H. Mikkelsen, *ACS Photonics*, 2018, **5**, 552–558.
- A. Venkatakrishnan, H. Chua, P. Tan, Z. Hu, H. Liu, Y. Liu, A. Carvalho, J. Lu and C. H. Sow, *ACS Nano*, 2017, **11**, 713–720.
- H. M. Oh, G. H. Han, H. Kim, J. J. Bae, M. S. Jeong and Y. H. Lee, *ACS Nano*, 2016, **10**, 5230–5236.
- J. Lu, A. Carvalho, X. K. Chan, H. Liu, B. Liu, E. S. Tok, K. P. Loh, A. H. Castro Neto and C. H. Sow, *Nano Lett.*, 2015, **15**, 3524–3532.
- Y. Yu, G. Li, L. Huang, A. Barrette, Y.-Q. Cai, Y. Yu, K. Gundogdu, Y.-W. Zhang and L. Cao, *ACS Nano*, 2017, **11**, 9390–9396.
- M. Amani, P. Taheri, R. Addou, G. H. Ahn, D. Kiriya, D.-H. Lien, J. W. Ager, R. M. Wallace and A. Javey, *Nano Lett.*, 2016, **16**, 2786–2791.
- A. Bera, D. V. S. Muthu and A. K. Sood, *J. Raman Spectrosc.*, 2018, **49**, 100–105.
- E. Kim, C. Ko, K. Kim, Y. Chen, J. Suh, S.-G. Ryu, K. Wu, X. Meng, A. Suslu, S. Tongay, J. Wu and C. P. Grigoropoulos, *Adv. Mater.*, 2016, **28**, 341–346.
- D.-H. Lien, S. Z. Uddin, M. Yeh, M. Amani, H. Kim, J. W. Ager, E. Yablonovitch and A. Javey, *Science*, 2019, **364**, 468–471.
- N. Kang, H. P. Paudel, M. N. Leuenberger, L. Tetard and S. I. Khondaker, *J. Phys. Chem. C*, 2014, **118**, 21258–21263.
- X. Zhang, X.-F. Qiao, W. Shi, J.-B. Wu, D.-S. Jiang and P.-H. Tan, *Chem. Soc. Rev.*, 2015, **44**, 2757–2785.
- F. Tumino, C. Grazianetti, C. Martella, M. Ruggieri, V. Russo, A. L. Bassi, A. Molle and C. S. Casari, *J. Phys. Chem. C*, 2021, **125**, 9479–9485.
- X. Zhang, H. Nan, S. Xiao, X. Wan, Z. Ni, X. Gu and K. Ostrikov, *ACS Appl. Mater. Interfaces*, 2017, **9**, 42121–42130.

- 34 K. Hao, J. F. Specht, P. Nagler, L. Xu, K. Tran, A. Singh, C. K. Dass, C. Schüller, T. Korn, M. Richter, A. Knorr, X. Li and G. Moody, *Nat. Commun.*, 2017, **8**, 15552.
- 35 J. Pei, J. Yang, T. Yildirim, H. Zhang and Y. Lu, *Adv. Mater.*, 2019, **31**, 1706945.
- 36 H. S. Lee, M. S. Kim, H. Kim and Y. H. Lee, *Phys. Rev. B*, 2016, **93**, 140409.
- 37 Z. Lin, B. R. Carvalho, E. Kahn, R. Lv, R. Rao, H. Terrones, M. A. Pimenta and M. Terrones, *2D Mater.*, 2016, **3**, 022002.